small methods
www.small-methods.com

An Integrated Droplet Manipulation Platform with Photodeformable Microfluidic Channels

*Quan Liu, Guodong Yu, Chongyu Zhu, Bo Peng, Ruohan Li, Tao Yi, and Yanlei Yu**

Manipulating droplets by light in microscale allows precise control of microfluidics, liquid delivery, micromachines, and so on. Among these applications, microfluidic technology is of particular interest for miniaturization of the portable analysis systems, which require the integration of various liquid operations in one device. Here, a photodeformable microfluidic platform is constructed by combining Laplace pressure and capillary condensation to integrate the transportation, fusion, separation, and mixing of liquid slugs in one chip. The Laplace pressure, attributed to the photodeformation of the liquid crystal polymers, is generated to propel the slug. The capillary condensation is introduced by the delicate design of the fluid channels, allowing the fusion and separation of slugs without any connected microvalves. Catalytic oxidation reaction and protein detection processes are realized in the platform, which are amenable to a variety of miniaturized bio-medical applications, such as portable analysis and point of care testing.

1. Introduction

Photo-induced manipulation of droplets is of considerably interest in microfluidics to perform the reactions and detections due to the remote and precise control of liquids in microscale.[1] The mechanisms of the previously reported photocontrolled droplet motion mainly focused on the Marangoni effect[2–6] or the wettability gradient.[7–10] For example, Faris et al. dispersed water droplets in decanol and used laser to create temperature gradient, which generated the Marangoni effect to drive the droplets.[3] Benito-Lopez and Diamond et al. dispersed oil droplets in water with surfactant. Marangoni effect was induced by the local polarity change of the photoresponsive surfactant molecules, resulting in the movement of the oil droplets.[4] Tang et al. used Marangoni effect to drive the liquid metal droplet in the surrounding liquid, which controlled the circuit[5] and the chaotic advection[6] in microscale. Jiang et al. used the microstructure of the solid surface to make the droplet produce asymmetric wettability, which caused the droplet to flow spontaneously on the solid surface.[9] Ichimura et al. used the *cis–trans* isomerization of azophenyl groups to change the surface polarity, moving oil droplets by wettability gradient.[10] However, these droplet motions were limited to relative low speeds and simple linear trajectories, which were undesirable for the reactions and detections in an integrated platform (at least involving liquid transportation, fusion, separation, and mixing).[11,12]

Recently, we presented a new way to manipulate droplets (liquid slugs) confined in a microtube by photo-induced asymmetric deformation. Photodeformable linear liquid crystal polymers (LLCPs) were chosen to fabricate the microtubes due to the excellent deformability and good processability for building 3D actuation structures.[13–15] Laplace pressure was generated when the microtubes deformed from cylinder-like to cone-like geometry attributed to the photoinduced orientation change of the liquid crystal units,[16–19] which led to the motion of the slug toward the narrower side. During the motion of the slug, mixing occurred simultaneously due to the formation of the vortex.[15] Furthermore, the fusion of two slugs was achieved in the junction of the Y-shaped tube. Although the slug transportation, mixing, and fusion have been realized individually in separated microtubes in the previous work, the integration of these operations in one platform has not been realized. The fused slug was "locked" in the junction, and was neither separated nor propelled by light. Therefore, the manipulation of the "locked" slug by light is crucial to the integration of other operations.

It has been reported that when two solid surfaces are lyophilic with respect to a vapor that is present in the intervening medium, the vapor will condense into a liquid phase if the gap between the two solid surfaces is sufficiently close, which is referred to as capillary condensation.[20] This phenomenon provides an excellent way to generate subtle connection of microscale liquids, which is formed spontaneously with several femtolitre (i.e., 10^{-15} L) in the gap.[21,22] If we can introduce the capillary condensation into the junction, a simple and straightforward method would be achieved to manipulate liquid fusion and separation. Owing to the capillary condensation and Laplace pressure, the integration of liquid transportation, fusion, and mixing in the chip is more than ever a realizable target.

Q. Liu, G. Yu, C. Zhu, B. Peng, Y. Yu
Department of Materials Science and State Key Laboratory of Molecular Engineering of Polymers
Fudan University
Shanghai 200433, China
E-mail: ylyu@fudan.edu.cn
R. Li, T. Yi
Department of Chemistry
Fudan University
Shanghai 200433, China

The ORCID identification number(s) for the author(s) of this article can be found under https://doi.org/10.1002/smtd.202100969.

DOI: 10.1002/smtd.202100969

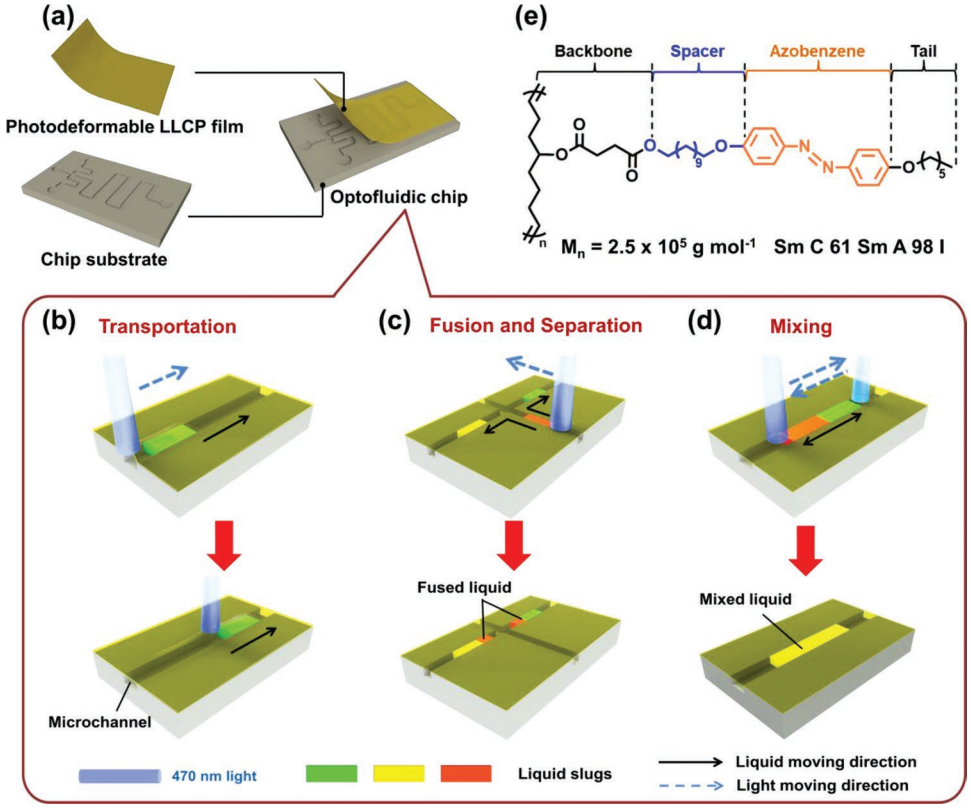

Figure 1. a) Schematics showing the fabrication of the photodeformable microfluidic chip by combining the photodeformable LLCP film and the substrate. b) Transportation of the slug in the chip with the light serves as a pump. c) Fusion and separation of two slugs in the chip with Y-shaped channel with the light serves as a valve. d) Mixing occurred in the slug by irradiating the two ends of the slug alternatively. e) Chemical structure of the photodeformable LLCP. M_n is the number-average molecular weight of the polymer. Sm C, Sm A, and I represent the smectic C phase, smectic A phase, and isotropic phase, respectively.

Here, we report an integrated droplet manipulation platform based on a photodeformable microfluidic chip, in which the transportation, fusion, and mixing of liquid slugs are controlled by the photo-induced Laplace pressure and the capillary condensation (**Figure 1**a–d). The Laplace pressure provides the driving force for the motion of the slugs, while the capillary condensation plays an important role in avoiding the "lock" of the fused slug in the microchannels, contributing to the integration of these liquid operations and the sequential control of reactions and detections in the same device. The photodeformable channels stimulated by a 470 nm light emitting diode (LED) source serve as pumps, valves, and mixers for all the liquid operations, completely removing the on-chip plumbing of conventional microfluidic chips (Figure S1, Supporting Information). This platform provides a new concept in the photocontrolled microfluidics, and lays the foundation of the portable analysis and point of care testing.

2. Results and Discussion

2.1. Design of the Photodeformable Microfluidic Chip

To construct the photodeformable microfluidic chip for integrating the transportation, fusion, separation, and mixing of the liquid slugs, at least two requirements need to be achieved: i) the microchannels are photodeformable to control the Laplace pressure. ii) the structure of the channels ensures the generation of the capillary condensation. Therefore, we prepared the film by using a photodeformable LLCP, which was synthesized by ring-open metathesis polymerization (Figure 1e; Scheme S1, Supporting Information). High-ordered lamellar mesophase and significant entanglement of polymer chains were formed due to the arrangement of the mesogens and the high molecular weight, acting as physical crosslinking to enhance the mechanical robustness and processability of the LLCP (Figure S2, Supporting Information).

Polymethyl methacrylate (PMMA) was chosen as the substrate material due to the high transparency and good processability. The isosceles trapezoidal microgrooves with a very small tilting angle λ (designed as 5°) were carved on the substrate by computerized numerical control (CNC) machine, which was elaborately designed and beneficial for the fusion and separation of the slugs (**Figure 2**a; Figure S3, Supporting Information). The photodeformable LLCP film bonded to the PMMA substrate tightly and seamlessly without using any glue because of the photoinduced solid-to-liquid transition effect.[23,24] After irradiated by UV light, the azobenzene moieties at the interface of the film closer to the substrate changed from *trans*-form to *cis*-form, which decreased the glass transition temperature (T_g)

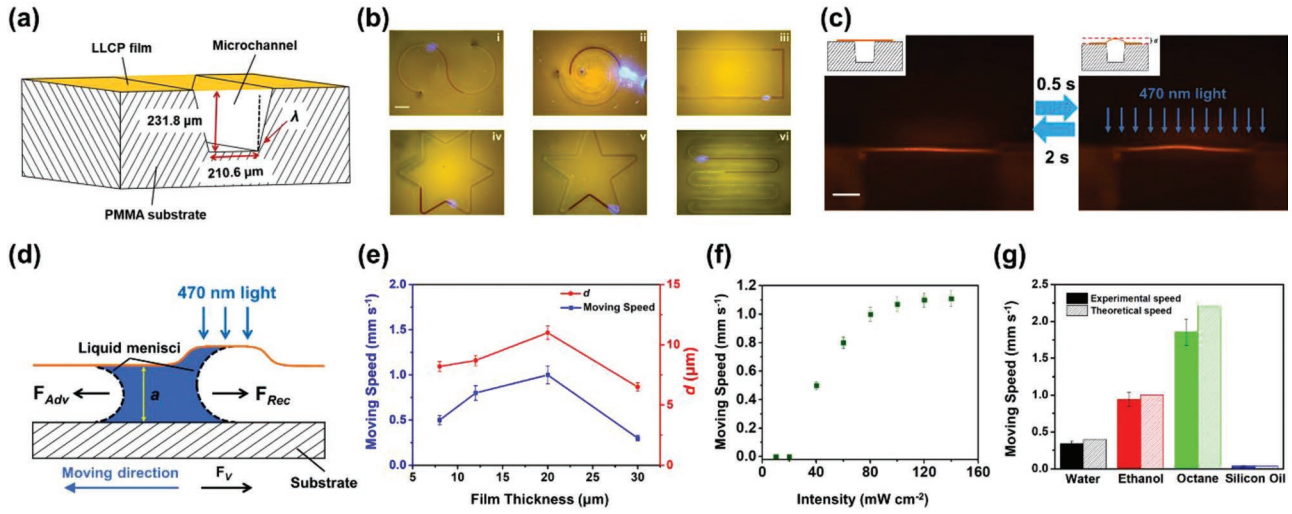

Figure 2. a) Schematic showing the cross section of the isosceles trapezoidal microgroove with a very small tilting angle λ. b) Top-view photographs of the photocontrolled slug motion in the i) S-shaped, ii) spiral-shaped, iii) right angle-shaped, iv) hexagram-shaped, v) pentacle-shaped, and vi) U-shaped continuous bent channels. The ethanol slug (dyed red), of which one side is irradiated by 470 nm light (80 mW cm^{-2}), moves away from the light source. The scale bar is 1 mm. c) Lateral view photographs of the LLCP film deformation upon irradiation of 470 nm light. The film bent to its maximum displacement within 0.5 s after exposure to the light, and return to its original shape within 2 s when remove the light. The inset pictures show the schematic of film deformation with the displacement of the film *d*. The scale bar is 50 μm. d) Schematic showing the force analysis during slug motion. e) Plot showing the relationship between the film thickness, the displacement of the film, and the moving speed of ethanol. The light intensity is 80 mW cm^{-2}. f) Plot showing the moving speed of ethanol increased with the increase of light intensity. The length of the ethanol slug tested in (e,f) is 0.5 mm. g) Plot showing the moving speeds of four kinds of liquid slugs under the same irradiation conditions: water (black solid column, 0.34 mm s^{-1}), ethanol (red solid column, 0.9 mm s^{-1}), octane (green solid column, 2.0 mm s^{-1}), and silicon oil (blue solid column, 0.04 mm s^{-1}). The values were achieved by testing the time taken for the liquid to move a certain distance. The twill columns show the theoretical speeds of the liquid slugs: water (0.4 mm s^{-1}), ethanol (1.0 mm s^{-1}), octane (2.2 mm s^{-1}), and silicon oil (0.04 mm s^{-1}). The volume of the liquids tested in (e–g) is 1 μm.

of this surface (from 35 to −29 °C, as seen in Figure S4, Supporting Information). The low-T_g surface turned into viscous flow state earlier, leading to the tight adhesion upon heating (Figures S5,S6, Supporting Information).

2.2. Photocontrolled Pumps for Liquid Slug Transportation

The photocontrolled motion of the liquid slug was then evaluated in the microfluidic chip. A liquid slug in the channel moved away from the irradiation point when one side of the liquid slug was irradiated by 470 nm blue light, and reversed the moving direction by altering the irradiation point to another side, as shown in Figure S7a and Movie S1, Supporting Information. The light spot followed the slug to generate partial expansion of the channel on one side of the slug. Liquid slugs were pumped by light not only in the straight channel, but also in the channel with complex shapes, including S-shape, spiral-shape, right angle-shape, hexagram-shape, and pentacle-shape (Figure 2b; Movie S2, Supporting Information). The motion of the slug in the various channels allows the integration of complex functions into a small region, such as a parallel liquid manipulation or a "micro pump" (Figure S7b,c, Supporting Information). The ethanol slug with length of 20 mm was manipulated to move more than 60 mm in the continuous U-shaped bent channels, and the whole moving process was observed in a visual field of 10 mm × 15 mm.

The driving force for the liquid slug motion is ascribed to the photo-induced capillary force arising from the asymmetric channel deformation of the two sides of the liquid slug. Upon irradiation of 470 nm blue light, the azobenzene moieties in the LLCP film were activated to repeat *trans–cis–trans* isomerization cycles (called Weigert effect),[25] causing the decrease of the order parameter and generating free-volume via oscillation of the azobenzene. In the case that the LLCP film was confined on the microgroove, the film expansion transmuted into cambered bending. The camber is convex rather than concave because the upper surface of the film is unfixed while the bottom surface of the film is subjected to the resistance from the substrate. As a result, the cross section area of the channel is increased (Figure 2c; Figure S8, Supporting Information). To make sure the deformation of the LLCP was mainly driven by photo-induced isomerization instead of photo-thermal phase transition, we tested the temperature change during the irradiation of the blue light by the infrared thermography. As shown in the Figure S9, Supporting Information, the temperature at the light spot increased only about 1 °C, which was too low to induce the phase transition of the LLCP for driving the deformation of the channel.

The displacement of the film (defined as the distance from the top of the camber to its original position, and represented by *d*) reached as large as 11 μm within 1 s after exposure to the light with the intensity of 80 mW cm^{-2}, and reversed to its original shape within 2 s when the light was removed (Figure 2c). The deformation and reversion process had no obvious fatigue even after 100 repetitions, showing the repeatable liquid slug control in the photodeformable channel (Figure S10, Supporting Information). The cross section area of the channel

changed attenuated along the length of the microgroove when one side of the liquid slug was irradiated. Since the slug moves away from the irradiation side owing to the partial expansion of the channel, we define the irradiation side of the slug as the "Receding Side" and the other side as the "Advancing Side." The radial surface tensions at two sides are F_{Adv} and F_{Rec}, leading to the formation of liquid menisci with different curvature radii, as shown in Figure 2d and Figure S11, Supporting Information. The completely wetting slug in the channel is subjected to two forces: the capillary driving force $F_c = F_{Adv} - F_{Rec}$ and the viscous force F_V, which opposes each other. In order to simplify the calculation, the isosceles trapezoidal cross section of the channel is considered as approximately square since the tilting angle λ is very small. Based on the Young–Laplace equation, the capillary driving force can be expressed as:

$$F_c = F_{Adv} - F_{Rec} \approx a\gamma Q \tag{1}$$

where a is the side length of the channel whose cross section is considered as square, γ is the surface tension of the slug, and Q is the deformation factor that relevant to the displacement of the film d: $Q = d/(2a + d)$. Meanwhile, the F_V can be expressed as:

$$F_V = 4\eta v l \tag{2}$$

where η is the dynamic viscosity of the slug, v is the average slug moving velocity, and l is the length of the slug. Therefore, the balance of the capillary driving force and the viscous force $F_c = F_V$ generates:

$$a\gamma Q \approx 4\eta v l \tag{3}$$

Considering the volume of the slug $\Omega = a^2 l$, the above equation is transformed to:

$$v \approx \frac{a\gamma Q}{4\eta l} = \frac{a^3 \gamma Q}{4\eta \Omega} \tag{4}$$

For ethanol with the volume of 1 µL, the dynamic viscosity η is 1 mPa·s (20 °C) and the surface tension γ is 20 mN m^{-1}. When d = 11 µm in the case that the light intensity is 80 mW cm^{-2} and the film thickness is 20 µm, we can get $Q = 2.5 \times 10^{-2}$. According to the equation above, $v \approx 1$ mm s^{-1}, which is close to the experimental result ($v_{exp} \approx 0.94$ mm s^{-1}).

According to the equation, the driving speed v is influenced by the displacement of the film (d) and the species of the slug (γ/η), where d is relevant to the film thickness and the light intensity. With the increase of the film thickness, the displacement increases at first and then decrease. It reaches the maximum value of 11 µm when the film thickness is 20 µm, leading to the moving speed of ethanol at about 1.0 mm s^{-1} (Figure 2e). The d increases with the increase of the light intensity, as shown in Figure S9, Supporting Information. The relationship between the moving speed and the light intensity is shown in Figure 2f. The moving speed of ethanol is enhanced to 1.1 mm s^{-1} with the light intensity of 140 mW cm^{-2}. Furthermore, the moving speed of different wetting slugs varies because of their different ratio of γ/η, the slug with higher γ/η moves faster when the other parameters (such as the film thickness, the light intensity, the slug volume, and the channel size) are remained constant. The moving speeds of four kinds of slug with the same volume (1 µL) are shown in Figure 2g, including water, organic solvent with different polarity, and polymer. The speed of octane, which is the highest among the four samples, reaches about 2.0 mm s^{-1} while that of the silicon oil is only 0.04 mm s^{-1}. For the slug that only partially wet the LLCP film or the PMMA substrate (such as water), the resistance generated by contact-line pinning was excluded through the coating a layer of hydrophilic nanoparticle-composite gel in the inner wall of the microchannel. (Figures S12,S13, Supporting Information). The moving speed of water reaches 0.34 mm s^{-1}, which satisfies the requirement for many biological applications with aqueous solutions such as the in-vitro detection[26] and the cell sorting.[27]

2.3. Photocontrolled Valves for Liquid Slug Fusion and Separation

To overcome the "lock" of the fused slug in the Y-shaped microchannels as found in our previous study,[11] the microgrooves were designed with isosceles trapezoidal cross section. With such design, a tiny connection was formed between the two liquid slugs (Liquid A in the left channel and Liquid B in the right channel) when they were driven to the junction point by 470 nm light. Upon irradiating the receding side of Liquid A, the slug transferred to the right channel and was fused with Liquid B through the tiny connection. The fusion stopped whenever the irradiation was removed, and the fusion direction was reversed when Liquid B was irradiated. When the junction point was irradiated, one part of the slug should move to the right channel and the other part should move to the left channel, so away from the irradiation point in both direction (**Figure 3**a).

During the fusion process, the two slugs are always independent except for the tiny connection on the margin of their menisci at the junction point. Mass transfer occurs from one slug to the other slug through the tiny connection, such as pouring the liquid in a tube along the margin of the tube. When the tiny connection is broken, the mass transfer stops and the two slugs are separated. The formation of the tiny connection arises from the capillary condensation due to the design of the isosceles trapezoidal cross section. As shown in Figure S15, Supporting Information, the intersection of the two trapezoidal channels results in the formation of tilted edge in the junction point. A wedge structure is comprised by the edge and the covered LLCP film. When the gap between the edge and the film is smaller than the critical radius of the concave R_k, the liquid is condensed in the tip of the gap due to the Kelvin Equation:

$$\frac{-0.414}{\log_{10}\frac{p}{p_0}} = R_k \tag{5}$$

where p is the vapor pressure of the concave, p_0 is the saturated vapor pressure. When the two slugs reach the junction point, the fusion and separation occur during the continuous irradiation of the receding side of Liquid A (Figure 3b,d): i) Liquid A moves in the branch channel until it reaches the

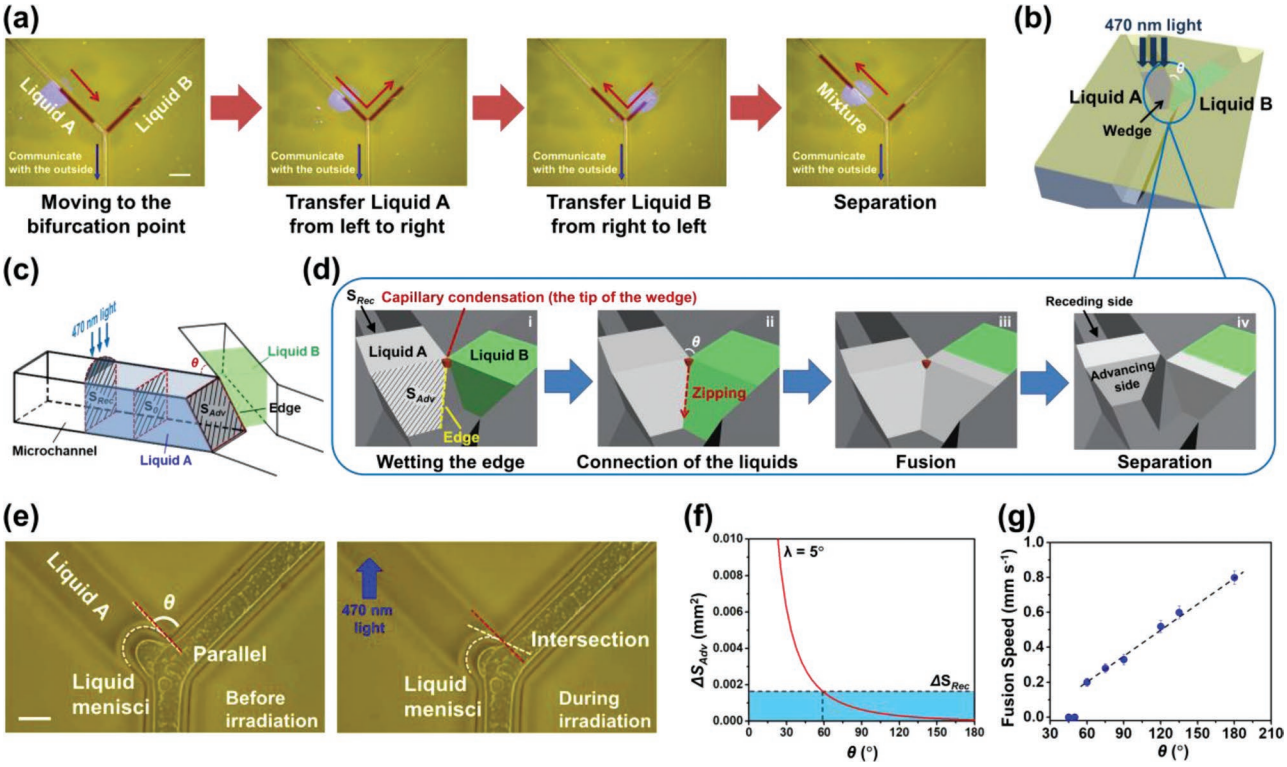

Figure 3. a) Photographs showing the fusion of two ethanol slugs (dyed red) in junction channels. The scale bar is 500 µm. b) schematics showing the Y-shaped channel with the trapezoidal cross section. A wedge structure is comprised by the edge and the covered LLCP film, and the angle between two branch channels is θ. c) Simulation of the fusion and separation of two slugs during irradiation. The cross section area of the microchannel is denoted by S_0, the receding side and advancing side of Liquid A by S_{Rec} and S_{Adv}, respectively. The angel between the two branch channels by θ. d) Schematics showing the process of the photocontrolled fusion. The fusion area is locally enlarged to show the details: i) The advancing side of Liquid A wets the edge (yellow dashed line) upon irradiation. Meanwhile, the capillary condensation is formed at the tip of the wedge (red block). ii) The capillary condensation acts as "zipper" to connect Liquid A and Liquid B (red dashed arrow). iii) Liquid A transfers to the neighboring channel and fuses with Liquid B. iv) The ebb of Liquid A and the separation of the two liquids after removing the irradiation. e) Variation of the meniscus of the liquid slug in the Y-shaped channel during the irradiation of the blue light. Before irradiation, the semicircular liquid meniscus at the advancing side of the slug is tangent to the edge. After irradiating the receding side of the slug, the liquid meniscus at the advancing side of the slug changes to arcuate and is intersected to the side wall of the groove. The scale bars are 200 µm. f) Plot showing the relationship between ΔS_{Adv} and θ. ΔS_{Adv} is the increased area of the advancing side after the liquid slug wetting the edge. g) Plot showing the relationship between the fusion speed of ethanol and θ. The film thickness is maintained 20 µm and the light intensity is 80 mW cm^{-2}.

junction point and is stopped by the edge, causing the increase of the cross-sectional area of the advancing side (S_{Adv}). Since the cross-sectional area of the receding side (S_{Rec}) is larger than S_{Adv}, the slug keeps moving tendency triggered by the Laplace pressure. Therefore, the liquid meniscus at the advancing side is intersection with the edge instead of parallel to the edge in the initial case (Figure 3e). ii) Under the interaction of the surface tensions of the two slugs on the edge, a connection across the edge is generated from the capillary condensation and realizes mass exchange, such as zipping clothes by the zipper. iii) Liquid A transfers to the neighbored channel and fuses with Liquid B gradually through the connection. iv) When the light is removed, S_{Rec} reverse to the original size of the channel, which is smaller than S_{Adv}. Thus the capillary force at the receding side is larger than that at the advancing side, causing the ebb of Liquid A and the separation of the fused slug. The ebbed Liquid A returns to the left channel and stops until S_{Adv} is equal to S_{Rec}, while the fused and separated slugs are moved for the further operations by light. Therefore, the fusion and separation of liquid slug in the chip is successfully manipulated by light without any other connected microvalves.

To further understand the above liquid slug fusion and separation behaviors, we calculated the change of the cross-sectional area during the whole process, which mainly controls the moving direction of the slug (due to the principle that the slug moves toward the narrow side controlled by Laplace pressure). According to the fusion mechanism, two factors are critical to the liquid connection: one is the generation of the capillary condensation; the other is the moving tendency when the slug is stopped by the edge. If the cross section of the channel is square, a vertical edge is formed, which provides no wedge structure to generate the capillary condensation. Besides, if the cross section of the channel is circle, the two cylindrical slugs fuse spontaneously and not reversible. Therefore, the tilting angle λ (as shown in Figure 2a) cannot be negligible and the cross section of the microchannel must be treated as isosceles trapezoidal. When the receding side of Liquid A is irradiated by the 470 nm light, the slug is driven

by the capillary force F_c, as mentioned in Equation (1). Q is the deformation factor that is relevant to the displacement of the film d:

$$Q \approx \frac{d}{100a + d} \approx \frac{S_{\mathrm{Rec}} - S_{\mathrm{Adv}}}{50a^2 + S_{\mathrm{Rec}} - S_{\mathrm{Adv}}} \tag{6}$$

We define $S_{\mathrm{Rec}} - S_0 = \Delta S_{\mathrm{Rec}}$, $S_{\mathrm{Adv}} - S_0 = \Delta S_{\mathrm{Adv}}$ (Figure 3c; Figures S14,S15, Supporting Information), then the Equation (1) can be expressed as:

$$F_{\mathrm{c}} = \frac{\Delta S_{\mathrm{Rec}} - \Delta S_{\mathrm{Adv}}}{50a^2 + \Delta S_{\mathrm{Rec}} - \Delta S_{\mathrm{Adv}}} a\gamma \tag{7}$$

According to the Laplace pressure driving principle, in order to maintain the moving tendency, the slug will move to the channel region with small cross section (narrow region) spontaneously, which means the cross-sectional area increment of advancing side ΔS_{Adv} need to be smaller than that of receding side ΔS_{Rec} when the slug is stopped by the edge. The detail of the fusion mechanism is discussed in the Supporting Information. ΔS_{Rec} is relevant to the photodeformation of the LLCP film, while ΔS_{Adv} is influenced by the tilting angle λ of the trapezoidal channel and the angle between two branch channels θ (Figure 3c; Figure S14,S15, Supporting Information). When the light intensity is 80 mW cm^{-2}, the LLCP film thickness is 20 μm, the d is 11 μm and the ΔS_{Rec} is calculated to be 0.0016 mm.[2] The ΔS_{Adv} scales as:

$$\Delta S_{\mathrm{Adv}} = S_0 \left(\sqrt{\frac{\tan^2 2\lambda}{\tan^2 \frac{\theta}{2}} + 1} - 1 \right) \tag{8}$$

where λ is the tilting angle of the isosceles trapezoidal microchannel, and θ is angle between the two branch channels. Therefore, the ΔS_{Adv} decreases with the decrease of λ, which means the fusion is easier to be realized with smaller λ.

When λ is fixed as 5°, ΔS_{Adv} decreases with the increase of θ and becomes smaller than ΔS_{Rec} until $\theta = 60°$, as shown in Figure 3f. The fusion occurs if θ is larger than 60° and accelerates with the increase of θ, which is ascribed to the increased moving tendency during the decrease of ΔS_{Adv} (Figure 3g; Movie S4, Supporting Information). After removing the irradiation on the receding side of Liquid A, the deformation of the LLCP film reverses to the flat state and $\Delta S_{\mathrm{Rec}} = 0$. In this case, F_{c} is reversed due to the ΔS_{Adv} larger than ΔS_{Rec}, leading to the ebb of Liquid A and the separation of the fused slug.

2.4. Photocontrolled Mixers for Liquid Slug Mixing

The fused liquid slugs were mixed rapidly after moving away from the junction without any mixers. We designed a neutralization reaction to demonstrate the photocontrolled mixing. As shown in Movie S5, Supporting Information, when the alkaline solution (dyed red by phenolphthalein) and the acid solution were fused and oscillated, the neutralization reaction occurred and the mixed liquid turned from red into colorless rapidly within 2 s. The fast mixing is ascribed to the formation of vortex during the capillary force-driven motion. As shown in Figure S16, Supporting Information, PS microparticles are dispersed in the slug. When the slug is driven by the photo-induced Laplace pressure, the vortex, demonstrated by the stirring of the PS microparticles, is formed during the motion of the slug. However, when the slug is driven by the syringe pump, the flow direction of the PS microparticles is parallel to the chip channel, which is caused by laminar flow. Hence, this chip requires neither mixing array-structures[28] nor micromachines[29] to realize photocontrolled mixing, and the mixing is accelerated by the photocontrolled oscillation of the slug.

A possible reason for the formation of the vortex is discussed below: The Laplace pressure is generated by the asymmetric surface tension on the contact line between the slug and the channel wall. Therefore, the flow rate from the surface to the core of the slug is non-uniform. The flow far away from the surface is dragged by the flow near the surface due to the viscosity of the slug, and induces the separation of the surface layer and the main stream. The liquid at the downstream of the separation point flows backward, leading to the formation of the vortex.

2.5. Photocontrolled Reaction and Detection in the Microfluidic Chip

The integration of the transportation, fusion, and mixing of the liquid slugs in the same device allows the simplification of biochemical analysis systems, in which the photodeformable channels act as all the pumps, valves, and mixers. We designed a microchannel network prototype for the reaction and detection, as shown in **Figure 4**a. The catalytic oxidation reaction of hydroxymethylfurfural (HMF) was taken as a model reaction in the chip, which was critically important as the product 2,5-furandicarboxylicacid (FDCA) had been receiving significant attention as a substitute for petrochemical-derived terephthalic acid in the synthesis of useful polymers (Figure 4b).[30] First, the preset HMF, NaOH, and tert-butyl hydrogen peroxide (TBHP) preinjected in the different channels were pumped to the junction point by light sequentially. Second, the three samples were fused together by the photocontrolled valve. Third, the fused samples were mixed uniformly during the oscillation of the irradiation. The whole photocontrolled reaction process is demonstrated in Figure 4c and Movie S6, Supporting Information. The reaction efficiency was tested by UV–vis spectra, as shown in Figure 4d. A significant increase of the absorption peak at 265 nm with time reflected the generation of FDCA. The concentration of FDCA was remarkably higher after 30 min reaction, which was much faster than that carried out in a flask (more than 24 h) due to the fully mixing in microscale by light.[31] Furthermore, the reaction of the fused samples was conducted by photo-induced oscillation in the channel with a length of ≈5 mm, which was much shorter than that in the other microfluidic chips only driving liquids toward one direction.[31]

In addition, we realized one-step detection of SIRT1, an important protein for neural plasticity and metabolic syndrome,[32] in the photodeformable microfluidic chip. The detection mechanism is shown in **Figure 5**a. The probe contains two fluorescent groups which are far away from each

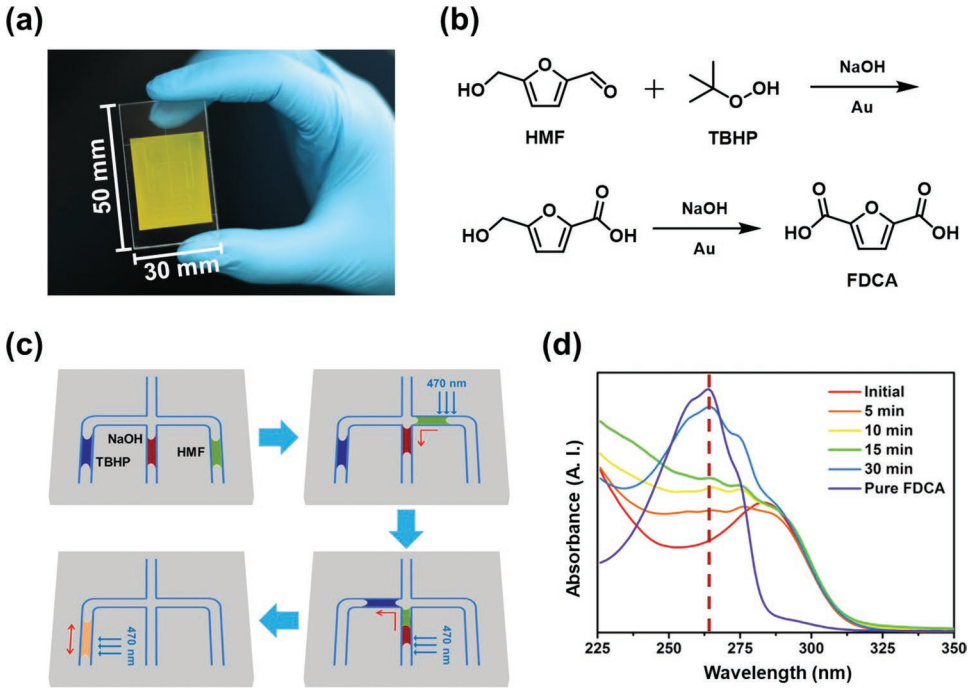

Figure 4. a) Photograph of the photodeformable microfluidic chip for the reaction and detection. b) The reaction formula of the catalytic oxidation of HMF. c) Schematics showing that upon irradiation of 470 nm light, the hydroxymethylfurfural (HMF) is fused with NaOH and tert-butyl hydrogen peroxide (TBHP) sequentially, and the fused liquid slugs are mixed uniformly. d) UV–vis spectra of the pure FDCA and the reaction mixture for different time. HMF shows an absorption peak at about 280 nm, while FDCA shows an absorption peak at about 265 nm.

other. After reacting with the protein, the distance between the two groups becomes narrow, which guarantees the energy transfer and emits fluorescence based on fluorescence resonance energy transfer (FRET). Here we preset 0.2 µL solution with and without SIRT1 in the left and right channel, respectively. 0.4 µL probe in the middle channel was separated into two parts and fused with the samples through photocontrol (Figure 5c). When the manipulation and the reaction was finished, the amide bond in the probe was digested by SIRT1, leading to an intramolecular rearrangement from the non-fluorescence oxy-benzoxadiazole group to green emissive nitro benzoxadiazole (NBD). Meanwhile, the distance between the energy donor NBD and the energy acceptor Cy5 group was close enough for the FRET effect (Figure 5b; Figure S17, Movie S7, Supporting Information).[33] Therefore, strong NIR fluorescence is shown in the confocal laser scanning microscopy (CLSM) imaging (Figure 5d, $\lambda_{ex} = 488$ nm). The sample volume is 2 orders of magnitude smaller than that in the conventional microfluidic chip (30 µL),[34] and the whole process is simpler than other protein detection methods such as enzyme linked immunosorbent assay to avoid false positive result.

3. Conclusion

In conclusion, photocontrolled transportation, fusion, separation, and mixing of the liquid slugs are integrated into one platform by combination of the photodeformation-induced Laplace pressure and the capillary condensation. The Laplace pressure is induced by the photodeformation of the LLCP film, while the capillary condensation is facilitated by the unique design of the channel with isosceles trapezoidal cross section in the substrate. The slug moving speed is determined by the displacement of the film and the species of the slug, which is calculated theoretically under the condition that the Laplace pressure is the driving force. In the fusion process, the isosceles trapezoidal channel ensures the moving tendency of the slug due to the asymmetric capillary forces caused by the $S_{Adv} < S_{Rec}$, while the formation of the capillary condensation overcomes the "lock" of the fused slug in the Y-shaped microchannels. The fusion in our chip stops whenever the irradiation is removed, and the fused slug can be separated and mixed uniformly by the generation of the vortex. Photodeformable channels act as pumps, valves, and other liquid controllers in this droplet manipulation platform, triggered by a 470 nm LED light source. Catalytic oxidation reaction and detection of protein are realized as model operations in the photodeformable microfluidic chip at first time, laying the foundation for miniaturized applications such as portable analysis and point of care testing.

4. Experimental Section

Materials: The experiment liquids and solvents were obtained from Sinopharm Chemical Reagent Co., Ltd. which included dichloromethane (99.5%), ethyl acetate (99.5%), petroleum ether (boiling range, 60–90 °C), octane (99.5%), and ethanol (99.5%). Deionized water was used for the measurements. Silicone oil (viscosity ≈10 mPa) was received from Aladdin Industrial Corporation. Sodium hydroxide (NaOH, 98%) was purchased from Sinopharm Chemical Reagent Co., Ltd. The PMMA substrates were achieved from Sandi New Material Co., Ltd. The CNC

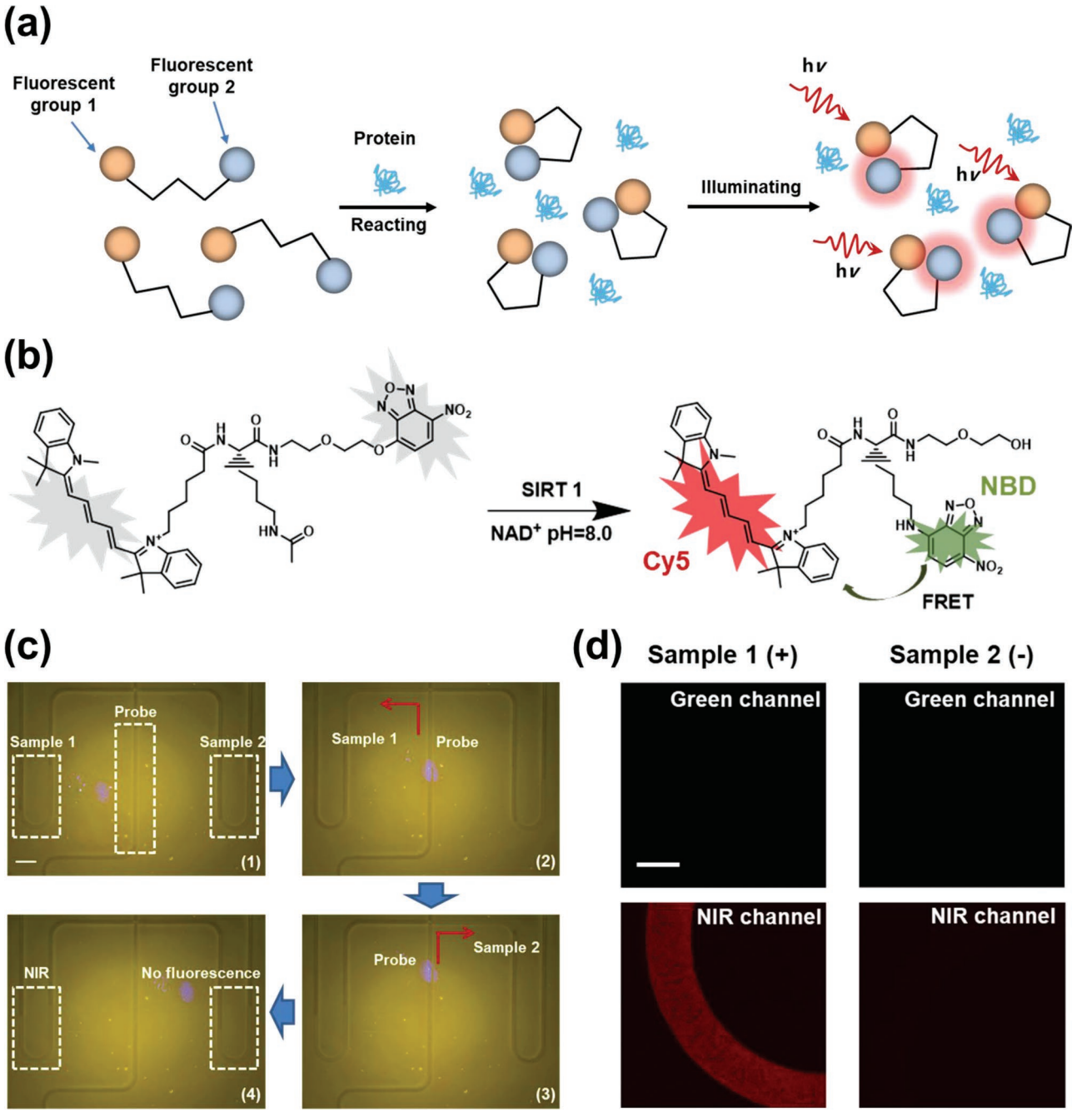

Figure 5. a) Schematics showing the mechanism of the FRET effect. b) The enzyme digestion reaction of the probe. Reproduced with permission.[33] Copyright 2019, Elsevier. c) Photographs showing the detection process. Upon irradiation by 470 nm light, the probe in the middle channel was separated into two parts and fused with the solution in the left (with SIRT1, Sample 1) and right channel (without SIRT1, Sample 2), respectively. The scale bar is 1 mm. d) CLSM images of Sample 1 and Sample 2 in the left and right channel of the chip, respectively. No signal is shown in the green channel while obvious fluorescence is shown in the NIR channel due to the energy transfer from NBD group to Cy5 group. Green channel: 520–560 nm, NIR channel: 620–690 nm, λ_{ex} = 488 nm. The scale bar is 200 μm.

mechining microknives (10°, 0.2 mm width) were purchased from Weitol Co., Ltd. The silicate composite nanoparticles solution (5–30 nm) was purchased from Hangzhou Wanjing New Material Co., Ltd. The reagents of the catalytic oxidation reaction and the neutralization reaction were purchased from Sigma Aldrich Reagent Co., Ltd. which included HMF, tert-butyl hydroperoxide solution (70% in water, Luperox TBH70X), and phenolphthalein. SIRT1 was purchased from Sigma Aldrich. Nicotinamide adenine dinucleotide (NAD^+) was purchased from Sangon Biotech (Shanghai) Co., Ltd. All chemicals were used as received without further purification.

LLCP Film Preparation: A solution of the LLCP in dichloromethane (2 wt%) was dropped on the glass substrate (30 mm × 40 mm) and the solvent was evaporated in the oven with 55 °C. Then, the formed film was peeled off from the glass substrate and the inhomogeneous edges were cut.

PMMA Substrate Fabrication: The PMMA sheet (30 mm × 50 mm) was washed by methanol twice and dried by nitrogen. The grooves designed

by Auto CAD were carved on the PMMA sheet by CNC machine with microknife (10°, 0.2 mm width). The grooved substrates were washed by toothbrush.

Construction of Photodeformable Microfluidic Chips: The chips were constructed by bonding of LLCP film and PMMA substrate. First, one surface of the LLCP film was irradiated by 365 nm UV light with the intensity of 50 mW cm^{-2}. After 10 min irradiation, the azobenzene moieties at the surface changed from *trans*-form to *cis*-form, which decreased the glass transition temperature (T_g) of this surface. Then the film was covered on the substrate with the irradiated surface touched the substrate. After heating at 105 °C for 2 min, the low-T_g surface turned into viscous flow state earlier, and bonded on the substrate tightly. Then the chip was cooled to 55 °C and annealed for 30 min, in order to facilitate the orientation of the mesogens.

The Catalytic Oxidization Reaction Experiment: The Au nanoparticles were deposited on the LLCP film and the grooves by Vacuum sputter evaporation technology. The current was set as 20 mA, and the deposition time was 60 s. After deposition of Au nanoparticles on the LLCP film and bonding of the chip, the microchannels were modified by applying a commercial silicate composite gel layer. In the reaction process, first the HMF (6 mM) in the left channel moved to the junction point and fused with NaOH (24 mM) in the middle channel. Then the TBHP (70% in water) in the right channel also moved to the junction point, and the three samples were fused together. The mixture was propelled to the U-shaped channel and oscillated for 30 min. Then the reacted solution was transferred to the cuvette for the UV–vis spectra investigation.

The FRET Experiment for Protein Detection: Two samples (named Sample 1 and Sample 2) and a probe solution were prepared before the protein detection experiment. Sample 1 was prepared by adding 7.54 µL SIRT1 in 100 µL HEPES buffer (pH = 8.0, containing 150 mM NaCl, 2.7 mM KCl, and 1 mM $MgCl_2$). Sample 2 was only HEPES buffer. The probe solution was prepared by adding 2 µL probe (0.3 mM in aqueous solution with 2% DMSO) and 4 µL NAD^+ solution in 100 µL HEPES buffer. 0.2 µL Sample 1, 0.4 µL probe solution and 0.2 µL Sample 2 were injected in the left, middle, and right channel, respectively. In the photocontrol process, first Sample 1 and probe solution were moved to the junction point, then about half of the probe solution was transferred to the left channel and fused with Sample 1. The last probe solution in the middle channel was fused with Sample 2 in the right channel. After fusing, the concentration of SIRT1 and the probe were 3.5 and 3 µM, respectively. The chip was sealed and the probe was incubated with SIRT1 at 37 °C for 2.5 h. After reaction, the enzymatic activity of SIRT1 was measured by CLSM imaging with excitation wavelength of 488 nm. A comparative reaction in micro-centrifuge tubes was performed with the same condition (same concentration of SIRT1, the probe, and NAD^+, same temperature, and time for reaction). The fluorescence signals were measured by a QM40 fluorescence photometer with excitation wavelength of 488 nm (Figure S17, Supporting Information).

Supporting Information

Supporting Information is available from the Wiley Online Library or from the author.

Acknowledgements

This work was supported financially from the National Natural Science Foundation of China (51927805, 21734003, and 52003055) and Innovation Program of Shanghai Municipal Education Commission (2017-01-07-00-07-E00027).

Conflict of Interest

The authors declare no conflict of interest.

Data Availability Statement

The data that supports the findings of this study are available in the supplementary material of this article.

Keywords

droplet manipulation, liquid crystal polymers, photocontrolled microfluidic chips, photodeformation

Received: August 18, 2021
Revised: October 23, 2021
Published online:

[1] R. Wang, K. Hashimoto, A. Fujishima, M. Chikuni, E. Kojima, A. Kitamura, M. Shimohigoshi, T. Watanabe, *Nature* **1997**, *388*, 431.
[2] C. Gao, L. Wang, Y. Lin, J. Li, Y. Liu, X. Li, S. Feng, Y. Zheng, *Adv. Funct. Mater.* **2018**, *28*, 1803072.
[3] K. Kotz, Y. Gu, G. Faris, *J. Am. Chem. Soc.* **2005**, *127*, 5736.
[4] L. Florea, K. Wagner, P. Wagner, G. Wallace, F. Benito-Lopez, D. Officer, D. Diamond, *Adv. Mater.* **2014**, *26*, 7339.
[5] H. Ren, H. Jin, J. Shu, J. Xie, E. Wang, D. Ge, S. Tang, X. Li, W. Li, S. Zhang, *Mater. Horiz.* **2021**, *8*, 3063.
[6] S. Tang, V. Sivan, P. Petersen, W. Zhang, P. Morrison, K. Kalantar-zadeh, A. Mitchell, K. Khoshmanesh, *Adv. Funct. Mater.* **2014**, *24*, 5851.
[7] P. Zhu, T. Kong, C. Zhou, L. Lei, L. Wang, *Small Methods* **2018**, *2*, 1800017.
[8] A. Diguet, R. Guillermic, N. Magome, A. Saint-Jalmes, Y. Chen, K. Yoshikawa, D. Baigl, *Angew. Chem., Int. Ed. Engl.* **2009**, *48*, 9281.
[9] C. Li, N. Li, X. Zhang, Z. Dong, H. Chen, L. Jiang, *Angew. Chem., Int. Ed.* **2016**, *55*, 14988.
[10] K. Ichimura, S. Oh, M. Nakagawa, *Science* **2000**, *288*, 1624.
[11] Y. Yang, Y. Chen, H. Tang, N. Zong, X. Jiang, *Small Methods* **2020**, *4*, 1900451.
[12] D. Baigl, *Lab Chip* **2012**, *12*, 3637.
[13] B. Xu, C. Zhu, L. Qin, J. Wei, Y. Yu, *Small* **2019**, *15*, 1901847.
[14] Q. Liu, Y. Liu, J. Lv, E. Chen, Y. Yu, *Adv. Intell. Syst.* **2019**, *1*, 1900060.
[15] J. Lv, Y. Liu, J. Wei, E. Chen, L. Qin, Y. Yu, *Nature* **2016**, *537*, 179.
[16] A. Gelebart, D. Mulder, M. Varga, A. Konya, G. Vantomme, E. Meijer, R. Selinger, D. Broer, *Nature* **2017**, *546*, 632.
[17] X. Qing, J. Lv, Y. Yu, *Acta Polym. Sin.* **2017**, *11*, 1679.
[18] X. Pang, J. Lv, C. Zhu, L. Qin, Y. Yu, *Adv. Mater.* **2019**, *31*, 1904224.
[19] C. Zhu, Y. Lu, J. Sun, Y. Yu, *Langmuir* **2020**, *36*, 6611.
[20] H. Butt, M. Kappl, *Adv. Colloid Interface Sci.* **2009**, *146*, 48.
[21] B. Bharti, D. Rutkowski, K. Han, A. Kumar, C. Hall, O. Velev, *J. Am. Chem. Soc.* **2016**, *138*, 14948.
[22] X. Tang, P. Zhu, Y. Tian, X. Zhou, T. Kong, L. Wang, *Nat. Commun.* **2017**, *8*, 14831.
[23] X. Qing, Y. Liu, J. Wei, R. Zheng, C. Zhu, Y. Yu, *Adv. Opt. Mater.* **2019**, *7*, 1801494.
[24] H. Zhou, C. Xue, P. Weis, Y. Suzuki, S. Huang, K. Koynov, G. Auernhammer, R. Berger, H. Butt, S. Wu, *Nat. Chem.* **2017**, *9*, 145.
[25] Y. Yu, T. Ikeda, *J. Photochem. Photobiol., A* **2004**, *5*, 247.
[26] T. Thomas, H. Unni, *Microfluid. Nanofluid.* **2019**, *23*, 105.
[27] X. Wang, S. Chen, M. Kong, Z. Wang, K. Costa, R. Li, D. Sun, *Lab Chip* **2011**, *11*, 3656.
[28] J. ter Schiphorst, G. Melpignano, H. Amirabadi, M. Houben, S. Bakker, J. Den Toonder, A. Schenning, *Macromol. Rapid Commun.* **2018**, *39*, 1700086.
[29] S. Neale, M. Macdonald, K. Dholakia, T. Krauss, *Nat. Mater.* **2005**, *4*, 530.

[30] Z. Zhang, K. Deng, *ACS Catal.* **2015**, *5*, 6529.
[31] C. Navin, K. Krishna, C. Theegala, C. Kumar, *Nanoscale* **2016**, *8*, 5546.
[32] W. Stunkel, R. Campbell, *J. Biomol. Screening* **2011**, *16*, 1153.
[33] R. Li, F. Xue, C. Cao, P. Wei, Y. Zhong, S. Xiao, F. Li, T. Yi, *Sens. Actuators, B* **2019**, *297*, 126791.
[34] Y. Liu, R. Gerber, J. Wu, T. Tsuruda, J. McCarter, *Anal. Biochem.* **2008**, *378*, 53.